Supplementary Information

Bonding-driven self-optimization of heterobilayer-passivated Cu–Cu interfaces for 3D integration

Jaewoon Koo[1†], Gun-Young Yoon[2†], Jimin Park[3†], Jungsoo Lee[1], Kyungjoon Kim[1], Minseong Ko[1], Myeongjae Heo[4], Gwangyu Kim[1], Myungho Choi[1], Heonjae Jeong[4,5*], Gangtae Jin[1*]

[1] Department of Semiconductor Engineering, Gachon University, Seongnam, 13120, South Korea

[2] Korea Institute of Materials Science, 797 Changwon-Daero, Seongsan-gu, Changwon, 51508, South Korea

[3] Department of Electronic Engineering, Gachon University, Seongnam, 13120, South Korea

[4] Department of Mechanical Engineering, Sogang University, Seoul 04107, South Korea

[5] Research Institute for Smart Design & Manufacturing Technology, Sogang University, Seoul 04107, South Korea

[†] These authors contributed equally: Jaewoon Koo, Gun-Young Yoon, Jimin Park

[*]Corresponding authors:

E-mails: hjeong@sogang.ac.kr, gjin@gachon.ac.kr

Supporting Figures

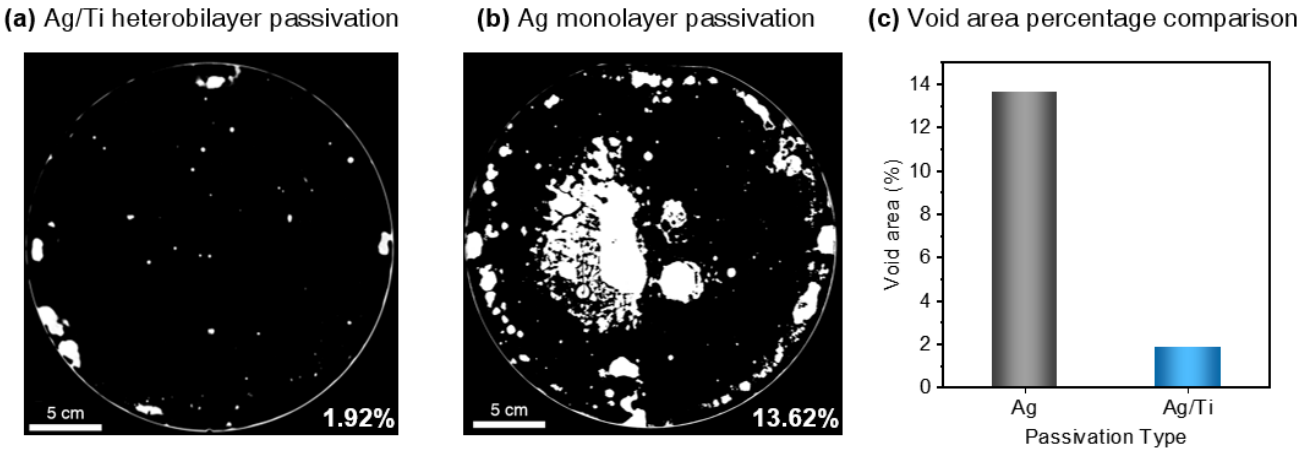

Figure S1. Quantitative void area percentage analysis of the bonded Cu–Cu interfaces via SAT C-scan imaging. (a) C-scan image of the bonded wafer with the proposed Ag/Ti heterobilayer passivation, exhibiting a void area percentage of 1.92%. (b) C-scan image with the conventional Ag monolayer passivation, exhibiting a void area percentage of 13.62%, and (c) Comparison bar chart of the calculated void area percentages between the two passivation results.

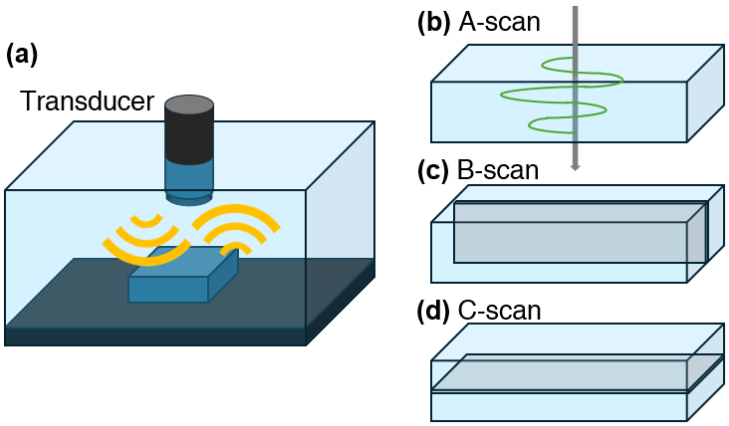

Figure S2. Scanning configurations and data acquisition modes of scanning acoustic tomography (SAT). (a) Schematic illustration of the ultrasonic transducer setup and acoustic wave propagation through a liquid coupling medium. (b) A-scan mode displaying a one-dimensional radio-frequency (RF) signal of echo amplitude versus time-of-flight at a localized coordinate for depth-resolved analysis. (c) B-scan mode providing two-dimensional vertical cross-sectional imaging to map internal structural continuity along a specific linear scan axis. (d) C-scan mode generating two-dimensional horizontal cross-sectional imaging at a gated depth for macroscopic void mapping and quantitative void ratio calculations.

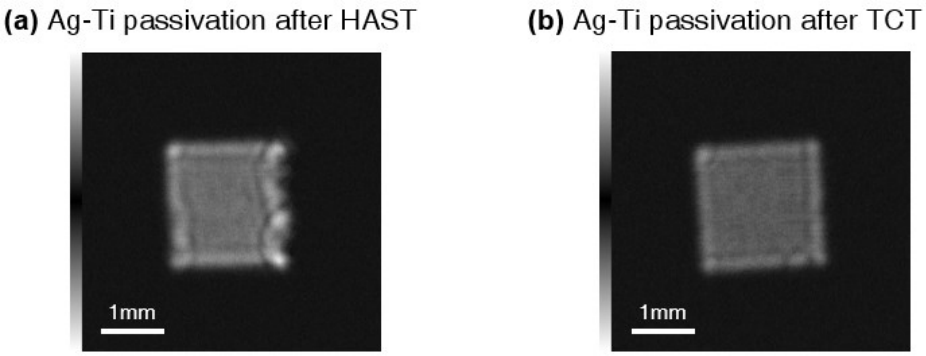

Figure S3. C-scan acoustic images of 2 mm diced bonded dies after post-environmental and thermomechanical stress tests (a) Ag/Ti passivation after HAST, (b) Ag/Ti passivation after TCT, illustrating the interfacial integrity and delamination behavior under accelerated aging conditions.

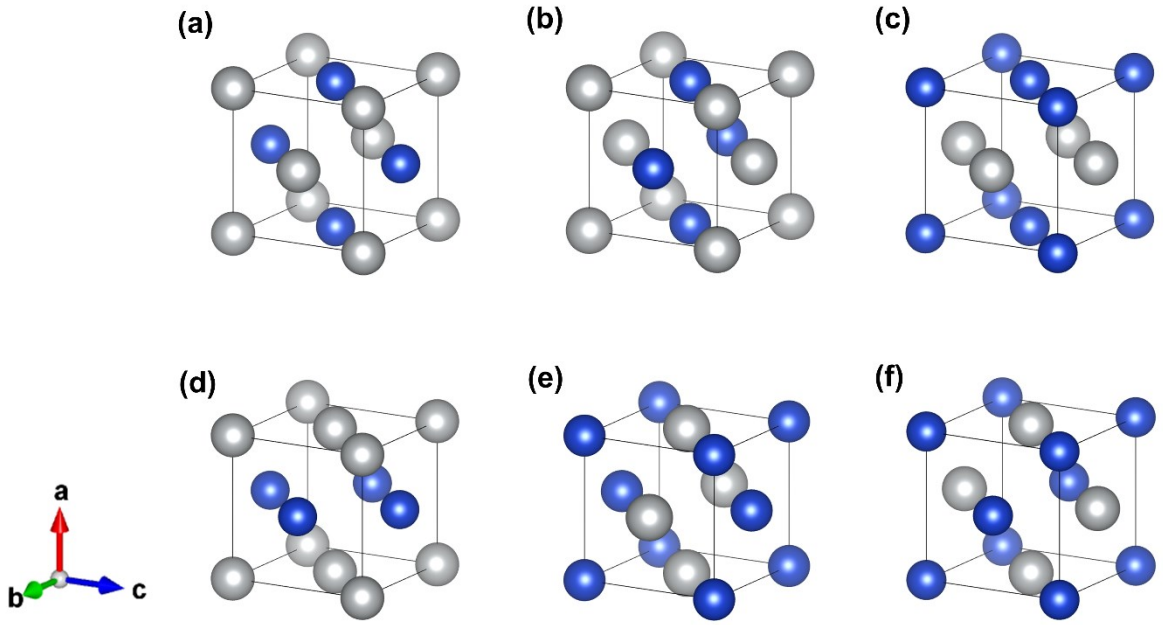

Figure S4. AgCu bulk structures with different atomic configurations. Panels (a-f) show the six inequivalent configurations considered in this study. Gray and blue atoms indicate Ag and Cu atoms.

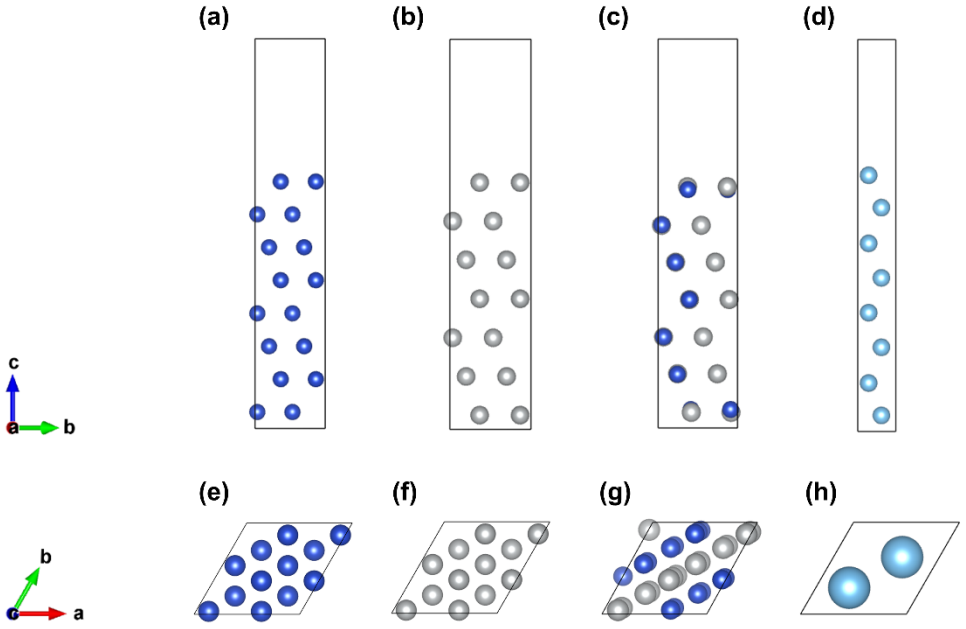

Figure S5. Crystal structures of the Cu(111), Ag(111), AgCu(111), and Ti(0001) slabs used in this study. (a-d) Side views and (e-h) top views of each slab, respectively.

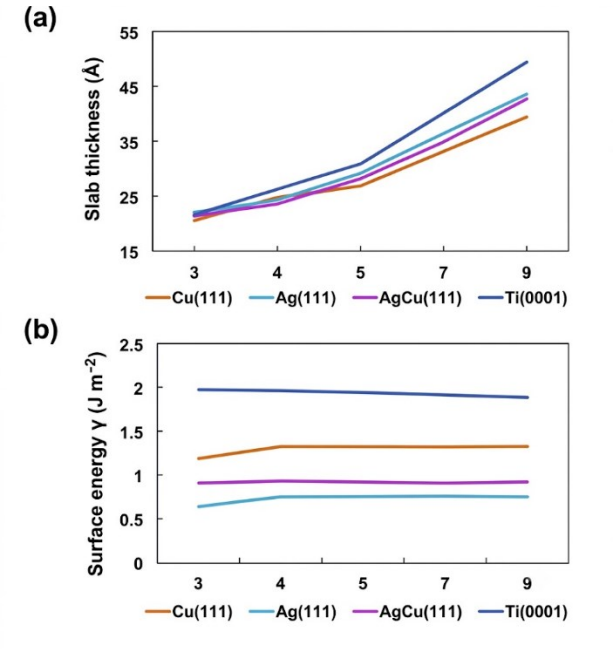

Figure S6. Convergence of (a) slab thickness and (b) surface energy with respect to the number of atomic layers (L) for the Cu(111), Ag(111), AgCu(111), and Ti(0001) slabs.

Supporting Tables

Table S1. Calculated interfacial energy (σ_{int}) and work of adhesion (W_{ad}) for the Ti(0001)/Cu(111), Ti(0001)/Ag(111), and Ti(0001)/AgCu(111) interfaces.

Interfacial model	Interfacial energy (J m^{-2})	Work of adhesion (J m^{-2})
Ti(0001)/Cu(111)	-0.79	4.01
Ti(0001)/Ag(111)	0.06	2.66
Ti(0001)/AgCu(111)	-0.36	3.20

Table S2. Integrated overlap area of the projected density of states (PDOS) at the Ti(0001)/Cu(111), Ti(0001)/Ag(111), and Ti(0001)/AgCu(111) interfaces.

Interfacial model	Overlapped d-orbital area (states)
Ti(0001)/Cu(111)	39.05
Ti(0001)/Ag(111)	12.51
Ti(0001)/AgCu(111)	13.64

Table S3. Number of atoms within the interfacial region for the Ti(0001)/Cu(111), Ti(0001)/Ag(111), and Ti(0001)/AgCu(111) interfaces.

Interfacial model	**N (A_N/B_N)**
Ti (0001) / Cu (111)	28 (Ti_{12}/Cu_{16})
Ti (0001) / Ag (111)	28 (Ti_{16}/Ag_{12})
Ti (0001) / AgCu (111)	28 (Ti_{16}/Ag_6Cu_6)

Table S4. Computational parameters used in the DFT calculations, including the plane-wave energy cutoff (E_{cut}), *k*-point meshes, and lattice parameters for the Cu, Ag, AgCu, and Ti bulk structures.

Bulks	**E_{cut} (eV)**	**k-points**	**Lattice parameter (Å)**		
			a	**b**	**c**
Cu	540	7 × 7 × 7	3.63	3.63	3.63
Ag	540	7 × 7 × 7	4.14	4.14	4.14
AgCu	540	7 × 7 × 7	3.83	3.95	3.95
Ti	540	9 × 9 × 4	2.93	2.93	4.61

Table S5. Calculated surface energies (γ) of low-index facets of Cu, Ag, AgCu, and Ti.

Slab	Surface orientation	Surface energy (J m^{-2})
Cu	(100)	1.46
	(110)	1.51
	(111)	1.19
Ag	(100)	0.80
	(110)	0.99
	(111)	0.64
AgCu	(100)	1.07
	(110)	1.07
	(111)	0.93
Ti	$(11\bar{2}0)$	1.86
	(0001)	1.94
	$(10\bar{1}0)$	2.24
	$(10\bar{1}1)$	1.97

Table S6. Slab thickness of the Cu(111), Ag(111), AgCu(111), and Ti(0001) slabs as a function of the number of atomic layers (L).

Atomic layers (L)	Slab thickness (Å)			
	Cu(111)	**Ag(111)**	**AgCu(111)**	**Ti(0001)**
3	20.49	21.96	21.29	21.57
4	24.68	24.22	23.55	26.20
5	26.78	29.14	28.07	30.83
7	33.07	36.32	34.85	40.09
9	39.37	43.50	41.63	49.35

Table S7. Calculated surface energies (γ) of the Cu(111), Ag(111), AgCu(111), and Ti(0001) slabs as a function of the number of atomic layers.

Atomic layers (L)	Surface energy (J m^{-2})			
	Cu(111)	Ag(111)	AgCu(111)	Ti(0001)
3	1.19	0.64	0.91	1.97
4	1.32	0.75	0.93	1.96
5	1.32	0.75	0.92	1.94
7	1.32	0.76	0.91	1.91
9	1.32	0.75	0.92	1.88

Table S8. Structural parameters of the lattice-matched Ti(0001)/Cu(111), Ti(0001)/Ag(111), and Ti(0001)/AgCu(111) interface supercells: total atom count (N) with a composition of A_N and B_N, interfacial area, and the in-plane lattice strain.

Interfacial model	**N (A_N/B_N)**	**Interfacial area (Å²)**	**Strain (%)**
Ti(0001)/Cu(111)	56 (Ti_{24}/Cu_{32})	22.45	0.61
Ti(0001)/Ag(111)	60 (Ti_{32}/Cu_{28})	29.93	0.86
Ti(0001)/AgCu(111)	60 (Ti_{32}/Cu_{28})	29.93	4.17

Table S9. Calculated cohesive energy (E_{coh}) of Cu, Ag, AgCu, and Ti bulk structures.

Bulk model	**E_{coh} (eV atom^{-1})**
Cu	3.49
Ag	2.52
AgCu	2.90
Ti	5.42

Table S10. Coefficients of determination (R^2) and diffusion coefficient (D) obtained from linear regression of the mean square displacement data for each atomic species at the Cu/Ti, Ag/Ti, and AgCu/Ti interfaces.

Atom(interface)	**R^2**	**D ($cm^2\ s^{-1}$)**
Cu(Cu/Ti)	0.64	1.57E-06
Ag(Ag/Ti)	0.78	1.11E-06
Ti(Cu/Ti)	0.95	5.39E-06
Ti(Ag/Ti)	0.96	2.42E-06
Cu(AgCu/Ti)	0.97	9.91E-06
Ag(AgCu/Ti)	0.98	3.93E-06
Ti(AgCu/Ti)	0.90	1.83E-06